NUMERICAL SIMULATIONS OF CRACK TIP STRESS-STRAIN FIELDS IN SINGLE CRYSTAL NICKEL-BASE SUPERALLOYS AT HIGH TEMPERATURE UNDER CREEP-FATIGUE LOADINGS

N. MARCHAL, S. FLOURIOT, S. FOREST, L. REMY
Centre des Matériaux, Ecole Nationale Supérieure des Mines de Paris – ARMINES - CNRS UMR 7633
BP 87, 91003 EVRY CEDEX, FRANCE

ABSTRACT

This work deals with the finite element analysis of cracks in single crystal Nickel-base superalloys. The first part consists in the computation of stress and strain fields at the tip of a static crack in a CT specimen. After a presentation of these crack tip fields in single crystals (Rice [1], Flouriot et al [2]), two-dimensional (001)[110] CT specimens subjected to creep-fatigue (mode I) loading are simulated. The slip systems activity at the crack tip is studied. The slip activity along the front localisation band is plotted as a function of the distance from the crack tip. Stress and strain are analysed at different points as a function of time. Then activity of slip systems is compared to the one obtained with pure creep or pure fatigue loadings, and the importance of dwell times is shown.

The second part deals with the influence of the wake plastic zone on the crack tip fields. The goal is to study the influence of precraking on the crack tip fields. The crack propagation is simulated using an uncoupled node-release technique. The load is calculated so that a decreasing ΔK is applied during precracking. Then, a monotonic loading is applied and the activity of slip systems is studied around the crack tip. This result is then compared to the one obtained without precracking.

This study of crack tip fields will contribute to the formulation of a crack propagation model based on local approach to fracture.

1 INTRODUCTION

Single crystal Nickel-base superalloys are used in aeroengines and gas turbines blades because of their high mechanical properties at high temperature and their good creep resistance. Theses blades are subjected to damaging thermo-mechanical creep-fatigue loadings that may result in the apparition of short cracks. A better understanding of crack propagation mechanisms in such single crystals is necessary because it should lead to improved life predictions and turbine performances.

In some temperature ranges, single crystal Nickel-base superalloys are prone to strain localization (Chieragatti [3], Hanriot [4]). This feature is thought to be very important in crack propagation. This is the reason why this paper focuses on phenomena occurring at the crack tip when the crack is subjected to mode I creep-fatigue loadings at high temperature (> 650°C). Then, it will focus on the influence of crack propagation on the crack tip stress and strain fields.

2 FINITE ELEMENT ANALYSIS OF CRACK TIP FIELDS UNDER CREEP-FATIGUE LOADINGS

In this part, 2D CT specimens are simulated, with the (001)[110] crack orientation ((001) is the crack propagation plane and [110] the crack propagation direction). After a presentation of the strain localization at the crack tip in single crystals and simulation conditions, the crack tip fields will be analyzed.

2.1 Strain localization at the crack tip and simulation conditions

Single crystal Nickel-base superalloys have a Face Centered Cubic crystallographic structure. Their plastic deformation is due to dislocations gliding on 12 octahedral and 6 cube slip systems.

2.1.1 Rice's solution

In single crystals the stress and strain fields in the vicinity of the crack tip are different from the ones of polycrystalline materials. In 1987, Rice (Rice [1]) found the asymptotic solution for a (001)[110] crack orientation, considering several assumptions: plane strain state, elastic-perfectly plastic material behaviour, mode I loading, monotonic loading.

This results in four sectors (A, B, C, D), in which the Cartesian components of stress are constant (figure 1). Between each sector, there is a strain localization band. The number of sectors/bands depends on crack orientation. So does the nature of the bands, which can be either slip bands, kink bands or multislip bands, depending on the orientation of the activated slip systems in the considered band with respect to the band direction. In the case of the (001)[110] crack orientation, there are three intense slip bands that form angles of 54.7°, 90° and 125.3° with the crack direction. The 54.7° and 125.3° bands are so-called slip bands, and they are due to octahedral slip, whereas the vertical band is a kink-band (figure 2), due to cube slip.

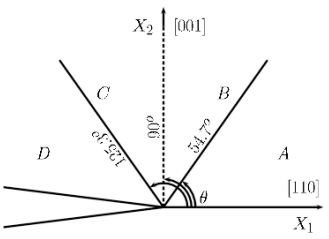

Figure 1 Constant stress sectors

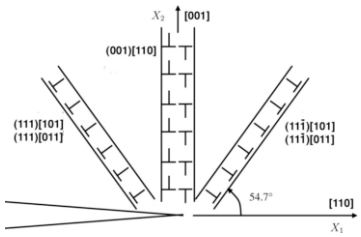

Figure 2 Nature of localization bands

In 1987, Saedvafa extended this asymptotic solution to power-law hardening materials (Saeedvafa and Rice [5]). An extensive study of crack orientations and localization patterns can be found in (Flouriot et al [2]). Finite Element simulations, as well as experimental observations, are consistent with these asymptotic solutions (Flouriot et al [2]). Rice's solution will be a guideline to understand the slip system activity in the coming sections.

2.1.2 The crystallographic model

The modelling of the material behaviour is done using Cailletaud's crystallographic model (Méric et al [6]). It consists in the description of the viscoplastic law at the slip system scale, the macroscopic deformation rate being obtained with the orientation tensor $\tilde{m}^s$:

$$\tilde{m}^s = \frac{1}{2}\left(\vec{n}^s \quad \vec{l}^s + \vec{l}^s \quad \vec{n}^s\right) \tag{1}$$

$$\dot{\underline{\underline{\varepsilon}}} = \dot{\underline{\underline{\varepsilon}}}_{oct} + \dot{\underline{\underline{\varepsilon}}}_{cub} = \sum_{s=1}^{12} \tilde{m}^s \dot{\gamma}^s_{oct} + \sum_{s=1}^{6} \tilde{m}^s \dot{\gamma}^s_{cub} \tag{2}$$

The flow rule on slip system s is: $\dot{\gamma}^s = \left\langle \frac{\left|\underline{\underline{\sigma}} : \tilde{m}^s - x^s\right| - r^s}{k} \right\rangle^n \operatorname{sgn}(\underline{\underline{\sigma}} : \tilde{m}^s - x^s)$ (3)

Isotropic hardening is considered constant: $r^s = r_0$ (4)

Kinematic hardening is non-linear: $x^s = c\alpha^s$ (5)

with $\dot{\alpha}^s = \dot{\varepsilon} - d\dot{v}^s \alpha^s$ where $\dot{v}^s = \left|\dot{\varepsilon}\right|$ (6)

This model was calibrated for AM1 and CMSX4 single crystals under cyclic loadings (Hanriot [4], Köster et al [7]).

2.1.3 Specimens geometries and loadings

The mesh is representative of CT specimens. Only one half of the specimen is meshed because of the problem symmetry. The calculation is done with plane strain conditions, to meet Rice's assumptions. The mesh consists of square quadratic elements around the crack tip (element size = 5 □m). The load ratio is R=0.1. Loading and unloading times are 1 s long, whereas the hold time is 90 s. K_{max} equals 20 $MPa\sqrt{m}$, which is a typical value for crack growth in superalloy single crystals. The coefficients of the constitutive law were chosen to simulate a high temperature behaviour with important viscous effects and significant hardening.

2.2 Simulation of 2D (001)[110] cracks

The finite element calculations are performed with the FE code Z-set, developed at Ecole des Mines de Paris, ONERA and Northwest Numerics (www.mat.ensmp.fr/Produits/Zebulon/index.html).

2.2.1 Isovalues of slip and activity of slip systems

On the following figures (3 to 5), the cumulated equivalent slip on octahedral systems is represented at three instants at the beginning of cycling. Instead of two localization bands at 54.7° and 125.3°, we can observe that sectors B and D (figure 1) are activated. This is due to the presence of a hardening term in the material model formulation. The vertical band, due to cube slip, is not represented here. The largest increase of slip is obtained during the first dwell time, whereas it seems to be much smaller during the second dwell period.

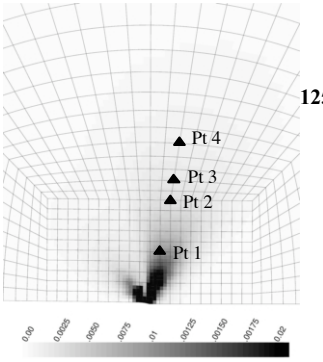

Figure 3□Beginning of the first dwell time

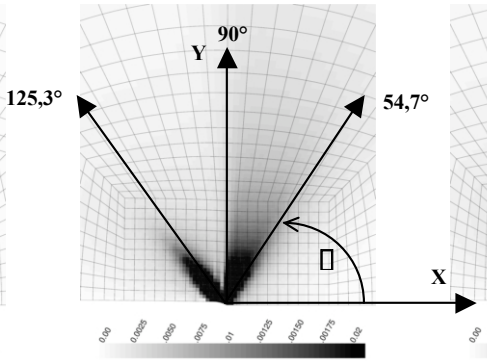

Figure 4□ End of the first dwell time

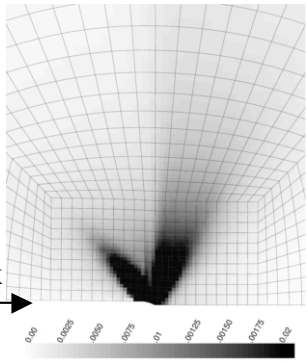

Figure 5□ End of the second dwell time

According to Rice's solution, the front band is due to the simultaneous and symmetrical activation of two octahedral slip systems $(11\bar{1})[101]$ and $(11\bar{1})[011]$, resulting in slip activity along a so-called effective slip system, $(11\bar{1})[112]$ (Flouriot et al [2]). This is the reason why only slip system $(11\bar{1})[101]$ will be considered in this part. Plotting the amount of slip along a path around the crack tip (distance: 35 □m) at the end of the first dwell reveals that the front band is oriented at approximately 70-80°.

The value of slip on system $(11\bar{1})[101]$ along this front band is represented on figure 6, as a function of time. The distances of points 1, 2, 3 and 4 from the crack tip are respectively 25, 50, 60 and 70 micrometers (figure 3).

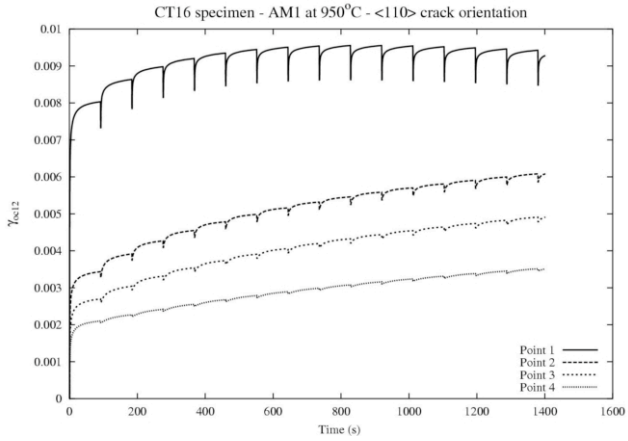

Figure 6 Amount of slip on system $(11\bar{1})[101]$ as a function of time, at points 1, 2 ,3, 4

The amount of slip increases during each cycle, up to a maximum for point 1, whereas the other points do not present such a stabilization of slip increase after 15 cycles. Concerning the resolved shear stress on the slip system, the stress relaxation after each loading tends to stabilize after 6 or 7 cycles at point 1, whereas the stress does not stabilize after 15 cycles for points 2, 3, and 4. These two phenomena can be seen on figure 7: the stress-strain loops represent the softening behaviour of the material. A local ratchetting effect can be observed on system $(11\bar{1})[101]$, which stabilizes for point 1 after 6-7 cycles, whereas there is no stabilization for points 2 to 4. Dwell time seems to be a key feature for the material behaviour, because of the important stress relaxation.

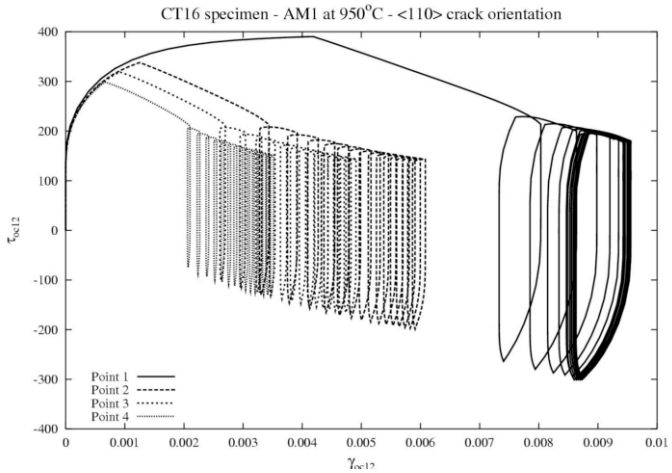

Figure 7 Resolved shear stress as a function of slip on system $(11\bar{1})[101]$

2.2.2 Comparison with pure fatigue and pure creep loadings

Pure fatigue loading (R=0.1, f=0.5 Hz, Kmax=20 $MPa\sqrt{m}$) and creep loading (K=20 $MPa\sqrt{m}$) were applied on the same specimen to compare slip systems activity for these different loadings. As shown on figure 8, rapid loading-unloading improves the amount of slip on the considered system during each cycle, up to a stabilized level after 6-7 cycles. Moreover, the comparison between pure fatigue loading and creep-fatigue reveals that dwell periods are very important for

stress relaxation, as shown on figure 9, where the maximum stress is much higher (280 MPa) after 6 fatigue cycles than after 6 creep-fatigue cycles (200 MPa).

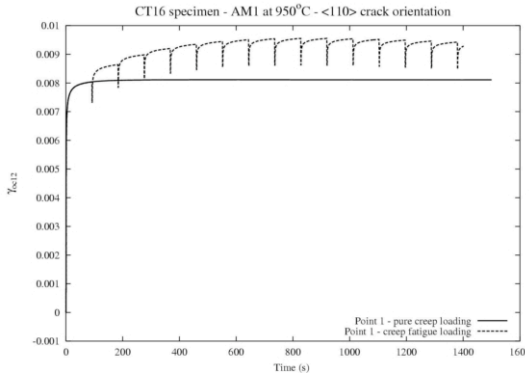

Figure 8 Slip on system $(11\bar{1})[101]$. Comparison between pure creep and creep-fatigue

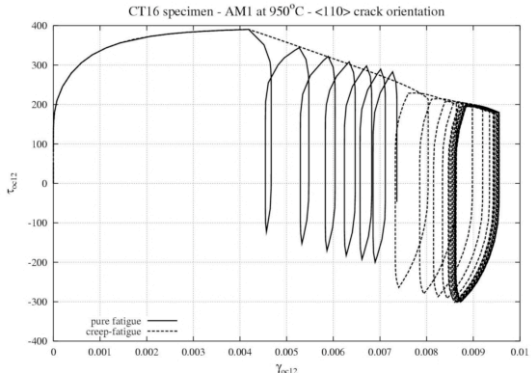

Figure 9 Stress-strain loops on system $(11\bar{1})[101]$. Comparison between pure fatigue and creep-fatigue

All these calculations were made on a "virgin" material, but real specimens are always precracked before testing. This is the reason why it is necessary to analyze the influence of the wake plastic zone on these fields.

3 INFLUENCE OF THE WAKE PLASTIC ZONE ON CRACK-TIP FIELDS

During precracking, the load is decreased step-by-step, so that the stress intensity factor decreases when the crack length increases. This allows getting the smallest possible plastic zone at the end of precracking. So, the crack propagation test begins with limited history effects. This is the reason why a linear function is introduced in the load calculation, so that the FE simulation can be as close as possible to the reality.

FE computations were performed using an uncoupled node-release technique. Each node is released after 4 cycles, the precracking distance being 0.4 mm. After crack propagation, a significant monotonic loading is applied, so that the end load is 3 times higher than the final precracking load.

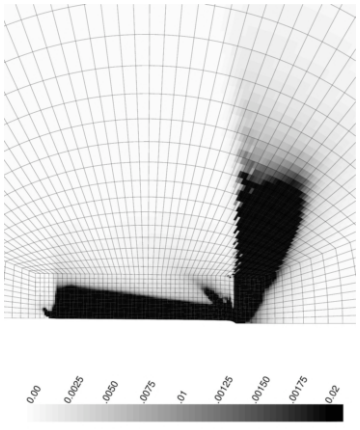

Figure 10 Octahedral cumulated slip at the end of the loading sequence

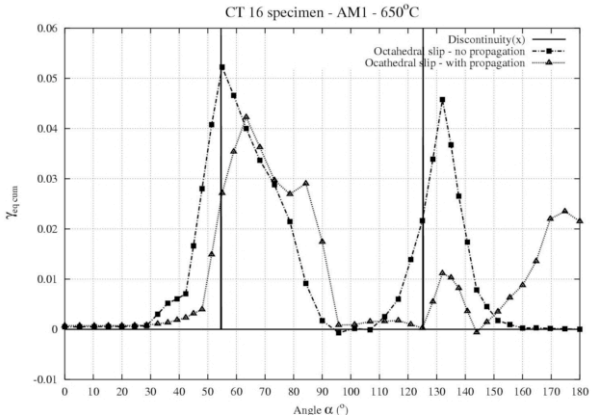

Figure 11 Comparison of octahedral slip between virgin and precracked specimens

Figure 10 shows the amount of cumulated octahedral slip at the end of the loading sequence. The crack propagated from the left to the right. On the left, a 125.3° strain localization band due to the beginning of precracking is visible. Then, the size of the activated zone decreases linearly, up to the right end, where the crack stops and the final loading is applied. The 54.7° and 125.3° localization bands are then visible.

It is then interesting to compare the slip systems activity with the one obtained just with a simple monotonic loading. This can be seen on figure 11, where the amount of cumulated slip at the end of the loading sequences is represented along a path that surrounds the crack tip (distance: 50 μm). We can see that the directions of the localization bands are almost the same if there is precracking or not. However, the slip intensity seems to be smaller for the precracked specimen than for the "virgin" one. Moreover, the influence of the wake plastic zone can be seen at 180° on this curve: in the case of precracking, the amount of slip is non-zero. This corresponds to the former activation of slip systems during crack propagation.

4 CONCLUSIONS

This study on crack tip stress and strain fields in single crystal Nickel-base superalloys reveals the importance of dwell times during loading. They enable important stress relaxation at the crack tip. Moreover, the wake plastic zone influences these crack tip fields: the orientation of the localization bands is not affected by former crack propagation, but the intensity of slip in these bands is changed. These phenomena are thought to be key features for crack propagation mechanisms in such materials. This study should lead to a local damage modelling for crack propagation.

5 ACKNOWLEDGEMENTS

The support of the European Commission in the framework of SOCRAX research project (G5RD-CT-2002-00819) is gratefully acknowledged by the authors.

6 REFERENCES

[1] Rice, J.R., *Tensile crack tip fields in elastic-ideally plastic crystals.* Mechanics of Materials, 6: p. 317-335. 1987.

[2] Flouriot, S., Forest, S., et al., *Strain localization at the crack tip in single crystal CT specimens under monotonous loading: 3D Finite Element analyses and application to nickel-base superalloys.* International Journal of Fracture, 124: p. 43-77. 2003.

[3] Chieragatti, R., *Influence of orientation on the low cycle fatigue behaviour of MAR-M200 single crystals. Part II: Cyclic stress-strain behaviour.* Materials Science and Engineering, A 141: p. 11-22. 1991.

[4] Hanriot, F., *Comportement du superalliage monocristallin AM1 sous sollicitations cycliques,* Ecole Nationale Supérieure des Mines de Paris. Ph.D. thesis. 119 pages. 1993.

[5] Saeedvafa, M. and Rice, J.R., *Crack tip singular fields in ductile crystals with Taylor power-law hardening. II: Plane Strain.* Journal of the Mechanics and Physics of Solids, 37 (6): p. 673-691. 1989.

[6] Méric, L., Poubanne, P., et al., *Single Crystal Modelling for Structural Calculations: Part 1 - Model Presentation.* Journal of Engineering Materials and Technology, 113: p. 162-170. 1991.

[7] Köster, A., Alam, A.M., et al., *A physical-base model for life prediction of single crystal turbine blades under creep-fatigue loading and thermal transient conditions*, in *Temperature-Fatigue interactions*, L. Rémy and J. Petit, Editors. ESIS Publication 29 - Elsevier, Paris. p. 203-212. 2002.